Deciphering the Cold Dense Matter EoS :

Integrating Nuclear Theory, Experiments and astrophysical Observations

Sk Md Adil Imam[1,2]*
[1]*Saha Institute of Nuclear Physics, 1/AF Bidhannagar, Kolkata 700064, India and*
[2]*Homi Bhabha National Institute, Anushakti Nagar, Mumbai 400094, India*

We implemented symbolic regression techniques to identify suitable analytical functions that map various properties of neutron stars (NSs), obtained by solving the Tolman-Oppenheimer-Volkoff (TOV) equations, to a few key parameters of the equation of state (EoS). These symbolic regression models (SRMs) are then employed to perform Bayesian inference with a comprehensive dataset from nuclear physics experiments and astrophysical observations. The posterior distributions of EoS parameters obtained from Bayesian inference using SRMs closely match those obtained directly from the solutions of TOV equations. Our SRM-based approach is approximately 100 times faster, enabling efficient Bayesian analyses across different combinations of data to explore their sensitivity to various EoS parameters within a reasonably short time.

Matter compressed to densities around and above the nuclear saturation density is widespread in the universe, found in atomic nuclei, neutron stars (NSs), and during core-collapse supernovae of massive stars. While the properties of dense strongly interacting matter are governed by quantum chromodynamics (QCD), but it is difficult to perform direct analytical and numerical QCD calculations [1, 2]. Therefore, understanding the properties of matter in the phase diagram of QCD remains an open problem in physics, necessitating effective theoretical approaches and empirical observations.

The equation of state (EoS), which describes the pressure-density-temperature relation of bulk matter, is the most fundamental macroscopic diagnostic of dense matter. The focus of the thesis is on the barotropic EoS, where pressure is solely a function of density independent of temperature. This EoS helps infer crucial aspects of microphysics, such as the role of many-body interactions at nuclear densities or the presence of deconfined quarks at high densities. The cold EoS is pivotal for determining the interior composition of isolated NSs [3, 4], understanding the tidal effects on gravitational wave (GW) signals from binary neutron stars (BNS) or neutron-star–black-hole binaries (NSBH) [5], and is intimately connected to the bulk properties of atomic nuclei [6].

Although our focus is on cold dense matter, it's worth noting that finite temperature effects on the EoS are relevant in various scenarios, such as the formation of proto-NSs immediately after core-collapse supernovae, nuclear collision experiments, the dynamics of compact binary coalescences involving NSs, and studies of the universe in its earliest stages. Investigating the dense matter EoS holds significant relevance for nuclear and astrophysical research, with profound theoretical implications for the nature of QCD matter [8].

Alternatively, one can impose limitations on the EoS by leveraging insights from microscopic theories, experimental data, and observations in astrophysics. However, when amalgamating nuclear and astrophysical data to deduce EoS properties, the analysis typically focuses on specific sources, and

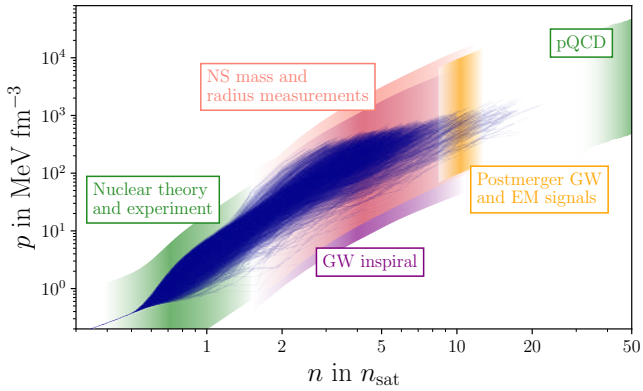

FIG. 1: Schematic overview of different sources of information about the dense matter EOS. The set of possible EOS candidates is shown by darkblue lines up to the respective maximum-mass configurations (TOV points). The colored bands roughly indicate the density regime where the different inputs constrain the EOS. It should be noted that the postmerger physics in BNS coalescences (orange band) depends also on finite-temperature effects of the EOS. This figure is taken from Ref.[7].

the individual impact of each measurement on the EoS and its parameter ranges is often overlooked. In this thesis, a wide-ranging, physics-agnostic prior for the dense-matter EoS is adopted and utilize a diverse array of nuclear and astrophysical constraints. The objective of the thesis is to investigate the distinct influences that each input exerts on the pool of potential EoS candidates. Employing a Bayesian approach, the posterior likelihood of the EoS for each constraint can be calculated, enabling one to set statistical boundaries on derived quantities like NS radii, and to compare the effectiveness of various observations in constraining the EoS. Furthermore, this methodology enables one to integrate different constraints in a coherent manner.

The constraints are investigated originate from diverse physical processes, thereby influencing the inference of the EoS across various density regimes. Fig. 1 shows a schematic

*Electronic address: mdadil.imam@saha.ac.in

overview at which regime a specific input constrains the EOS. The overarching properties of neutron stars (NSs), such as their masses, radii, and tidal deformabilities, primarily reflect the core of the star, where densities of several ρ_0 are attained, thereby constraining the EOS up to this density regime[9]. As densities reach around 40 ρ_0, quantum chromodynamics (QCD) transitions into a perturbative regime, allowing for direct analytical calculations of quark matter and offering insights into the density-pressure relation, which further informs the EOS at NS densities [10]. Given this broad density range, our objective is to incorporate a plethora of constraints from both astrophysics and nuclear physics, encompassing the entire EOS spectrum. However, it should be mentioned that not all constraints discussed in the literature are included in this thesis. The core region of a NS, characterized by densities above $0.5\rho_0$, is typically assumed to consist of nucleons, electrons, and muons. The energy per nucleon for neutron star matter, denoted as $\varepsilon(\rho, \delta)$, at a given total nucleon density ρ and asymmetry δ, can be broken down into two components: the energy per nucleon for symmetric nuclear matter (SNM), denoted as $\varepsilon(\rho, 0)$, and the density-dependent symmetry energy represented by $J(\rho)$ in a parabolic approximation as,

$$\varepsilon(\rho, \delta) \;=\; \varepsilon(\rho, 0) + J(\rho)\delta^2 + ..., \tag{1}$$

where, $\delta = \left(\frac{\rho_n - \rho_p}{\rho}\right)$ with ρ_n and ρ_p being the neutron and proton densities, respectively. The asymmetry parameter δ at a given density ρ is determined by satisfying the conditions of β-equilibrium and charge neutrality. Once δ is established, the proportions of neutrons, protons, electrons, and muons can be readily calculated. For densities below $0.5\rho_0$, a neutron star is characterized by an outer and inner crust. The EoS for the outer crust, encompassing up to $0.00016\rho_0$, is derived from the work by [11], while a polytropic form of the EoS, as described in [12], is adopted for the inner crust. These EoS formulations are employed in determining neutron star properties through the solutions of the Tolman-Oppenheimer-Volkoff (TOV) equations [3]. Each EoS model must adhere to the following criteria: (i) Mechanical stability ($c_s^2 \geq 0$), (ii) Causality ($c_s^2 \leq 1$), (iii) Positive symmetry energy, and (iv) A maximum neutron star mass, denoted as M_{TOV}, exceeding 2.0 times the solar mass ($M_\odot$). Here, c_s represents the speed of sound in units of the speed of light. In our studies, four types of EoS models are considered : (i) Taylor Expansion, (ii) $\frac{n}{3}$ Expansion, (iii) Skyrme based non-relativistic, and (iv) Relativistic Mean Field (RMF) models.

To reconstruct the EoS in a Bayesian approach pseudo data sets are generated using Taylor and $\frac{n}{3}$ expansion [13]. An initial set of NMPs are chosen to generate the mock data and for the Bayesian inference a suitable priors are chosen for each of the NMPs. From the posterior distribution of the NMPs it is found that the uncertainties on the higher order NMPs are very large. These uncertainties arises due to the correlation between the NMPs. The results are plotted for the $\frac{n}{3}$ expansion in Fig. 2. The value of $\varepsilon(\rho, \delta)$ (top) vary in a narrow bound at a given density, but, $\varepsilon(\rho, 0)$ (middle) and $J(\rho)$ (bottom) have larger uncertainties. The larger spread in $J(\rho)$

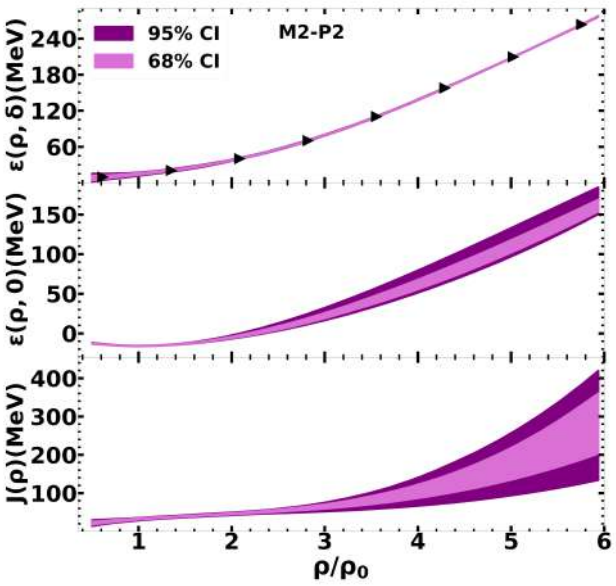

FIG. 2: Plots of 68% and 95% confidence intervals for the EoS for neutron star matter (top), the symmetric nuclear matter (middle), and the symmetry energy (bottom) as a function of scaled density for model M2 with prior set P2. The results are obtained from the posterior distributions of the NMPs which are reconstructed from the pseudo data for the EoS of neutron star matter(triangles). The spread in $\varepsilon(\rho, 0)$ and $J(\rho)$ are consistent with those for $\varepsilon(\rho, \delta)$.

is balanced by asymmetry parameter δ as well as by change in $\varepsilon(\rho, 0)$ such that the EoS for neutron star matter remains almost unaffected. The value of asymmetry parameter δ is mainly governed by the symmetry energy at a given density. As the symmetry energy increases, the δ decreases. Thus, the symmetry energy and δ may balance each other in such a way that the asymmetric part of the EoS of neutron star matter remains unaffected. Moreover, the variations in the asymmetric part of $\varepsilon(\rho, \delta)$ may also be compensated by the symmetric nuclear matter $\varepsilon(\rho, 0)$. In short, for a given $\epsilon(\rho, \delta)$, the values of $J(\rho)$, $\varepsilon(\rho, 0)$ and δ may have some leeway. Hence the EoS of neutron star matter alone may not be sufficient to determine the higher-order NMPs in narrow bounds. The higher-order NMPs are correlated to the lower-order ones, thus, the low-density ab-initio predictions for the EoS of symmetric nuclear matter and pure neutron matter from the chiral effective field theory should also be considered for the improved parameterizations. The experimental data on the EoS of symmetric nuclear matter from the heavy-ion collision and the symmetry energy beyond the saturation density from the isobaric analog states may further help in constraining the nuclear matter parameters.

To address the issue above a comprehensive set of data from nuclear experiments and astrophysical observations are utilized to constrain the NMPs and hence the EoS[14]. To per-

form the analysis relativistic and non-relativistic mean-field models are used to calculate the properties of nuclear matter at several densities and the EoSs for the neutron star matter [14]. The properties of nuclear matter considered are the pressure for the symmetric nuclear matter ($P_{\rm SNM}$), symmetry energy pressure ($P_{\rm sym}$) and the symmetry energy ($e_{\rm sym}$) which are constrained empirically over a range of densities by the experimental data on bulk properties of finite nuclei such as the nuclear masses (2), neutron skin thickness in ^{208}Pb (1) and the dipole polarizability (1), isobaric analog states (1) as well as the HIC data (7) spanning the density range 0.03 - 0.32 fm^{-3}, where the number of data points for a given quantity has been indicated in the parentheses. The astrophysics data considered are the radii of neutron stars with masses around the canonical one and ~ 2.1 M$_\odot$, the dimensionless tidal deformability for the neutron star around the canonical mass and the current bound on the maximum mass of the neutron star. The EoSs are subjected to these constraints within the Bayesian framework. The distributions of the nuclear matter parameters for the Skyrme model are relatively wider compared to those for the RMF models. It may be emphasized that the values of nuclear matter parameters obtained from the Skyrme and RMF models differ significantly, despite being inferred from the same data set. For instance, the median value for K_0 is higher in the Skyrme model by about 20% compared to the RMF model, while the median value of L_0 in the Skyrme model is lower by the same amount. This suggests that the Skyrme model yields a stiffer EoS for symmetric nuclear matter around $\sim \rho_0$, but with a softer density-dependent symmetry energy. Further L_0 exhibits correlations with J_0 and $K_{\rm sym0}$ for both the models. However, the strength of correlations between the remaining pairs of nuclear matter parameters are relatively weaker. In the case of the Skyrme model, the correlations between L_0 and $K_{\rm sym0}$ with $R_{1.4}$ and $\Lambda_{1.36}$ appear relatively stronger compared to those in the RMF model.

In the left panel of Fig.(3), the 95% confidence intervals represent the updated EoSs achieved by sequentially incorporating the constraints. The original priors (grey band) are also depicted for comparison purposes. The maximum NS mass significantly constrains the EoSs (empty blue band) which further narrow down with the inclusion of experimental data (magenta band). The introduction of constraints from astrophysical observations does not notably impact the EoSs. The Kullback-Liebler divergence (D_{KL}) provides a quantitative comparison between two different distributions. The D_{KL} comparing distributions P and Q is defined as,
$D_{KL}(P||Q) = \int_{-\infty}^{+\infty} P(x)\log_2(\frac{P(x)}{Q(x)})dx$. For a more detailed comparison, the D_{KL} as a function of baryon density for two distributions of the EoSs corresponding to different scenarios is evaluated. In the right panel of Fig.(3), the solid lines represent the value of D_{KL} obtained by comparing the distributions of EoSs between "$M_{\rm max}$" and "$M_{\rm max}$ + EXPT" scenarios. Similarly, the dashed lines represent the value of D_{KL} obtained by comparing the distributions of EoSs between "$M_{\rm max}$" and "ALL" scenarios. The values of D_{KL} for the solid lines indicate that the experimental data provides tighter constraints on the EoS in the vicinity of ρ_0. The proximity between solid and dashed lines indicates that including astrophysical observations does not impose stricter constraints beyond those set by the experimental data. However, the presence of a minor peak around 2-3ρ_0 in both models suggests that astrophysical observations on NS radii and tidal deformability introduce additional constraints within this density range.

The objective of this chapter is to identify the subset of the NMPs on which the tidal deformability predominantly depends over a range of NS mass relevant for astrophysical observations of BNS events detectable in the near future. In this context, the dependencies of Λ on the NMPs in the form of simple polynomial series of those predominant is studied parameters. Such mapping would enable us to evaluate Λ without recourse to the computationally expensive solutions of the TOV equations which will pave the way for the Bayesian parameter estimation of the NMPs from the GW events in a computationally efficient method. A large number of EoSs ($\approx 10^4$) are constructed by drawing all the nine NMPs randomly from their uniform probability distributions [15] to compute tidal deformability (Λ_{TOV}(M)) from the solutions of the TOV equations at a given NS mass M. In the upper panel of Fig.4, the correlations between Λ_{TOV}(M) and the pressure of β-equilibrated matter across various densities spanning from 0.5 - 4ρ_0 are displayed. This investigation extends to assessing the correlations between the NMPs and the pressure of β-equilibrated matter at a specific density, depicted in the lower panel of the figure. The NMPs L_0, $K_{\rm sym0}$, Q_0 and K_0 shows stronger correlation with pressure at the density range where tidal deformability shows the strongest correlation with pressure. The remaining NMPs exhibit negligible correlations with pressure, indicated by coefficients $r \leq 0.1$. So the tidal deformability for a given NS mass using linear (Λ_{l_n}) and quadratic (Λ_{q_n}) functions of n number of NMPs is expressed as

$$\Lambda_{l_n} = c_0 + \sum_{i=1}^{n} c_i(x_i - \hat{x}_i) \quad (2)$$

$$\Lambda_{q_n} = \Lambda_{l_n} + \sum_{i=1}^{n}\sum_{j=i}^{n} c_{ij}(x_i - \hat{x}_i)(x_j - \hat{x}_j) \quad (3)$$

where, $x \in \{e_0, K_0, Q_0, Z_0, J_0, L_0, K_{\rm sym0}, Q_{\rm sym0}, Z_{\rm sym0}\}$ for $n = 9$; and $\hat{x}$ corresponds to the median value of parameter x. The coefficients c_i and c_{ij} are obtained by fitting the values of Λ_{TOV}(M) to the Eqs. (2) and (3). Here Λ_{l_n}, Λ_{q_n} with $n = 2$ and $n = 4$ which correspond to $x \in \{L_0, K_{\rm sym0}\}$ and $x \in \{K_0, Q_0, L_0, K_{\rm sym0}\}$, respectively. The Λ_{l_9} which includes all the nine NMPs and $\Lambda_{q_4+l_5}$ with q_4 denotes contribution up to quadratic order for $x \in \{K_0, Q_0, L_0, K_{\rm sym0}\}$ and l_5 denotes the linear contributions from the remaining 5 NMPs are also considered. Various Λ_{func} are constructed by employing different combinations of NMPs and correlations between Λ_{func} and Λ_{TOV} are computed. The functions exhibit the most robust correlations with Λ_{TOV}(M) are Λ_{l_9} ($r \geq 0.95$) and $\Lambda_{q_4+l_5}$ ($r > 0.98$).

The ratio , $\mathcal{R}_M = \frac{\Lambda_{TOV}(M)}{\Lambda_{func}(M)}$ for the NS masses 1.2 M$_\odot$ - 1.8 M$_\odot$ for three different sets of NMP computed are : (i) with

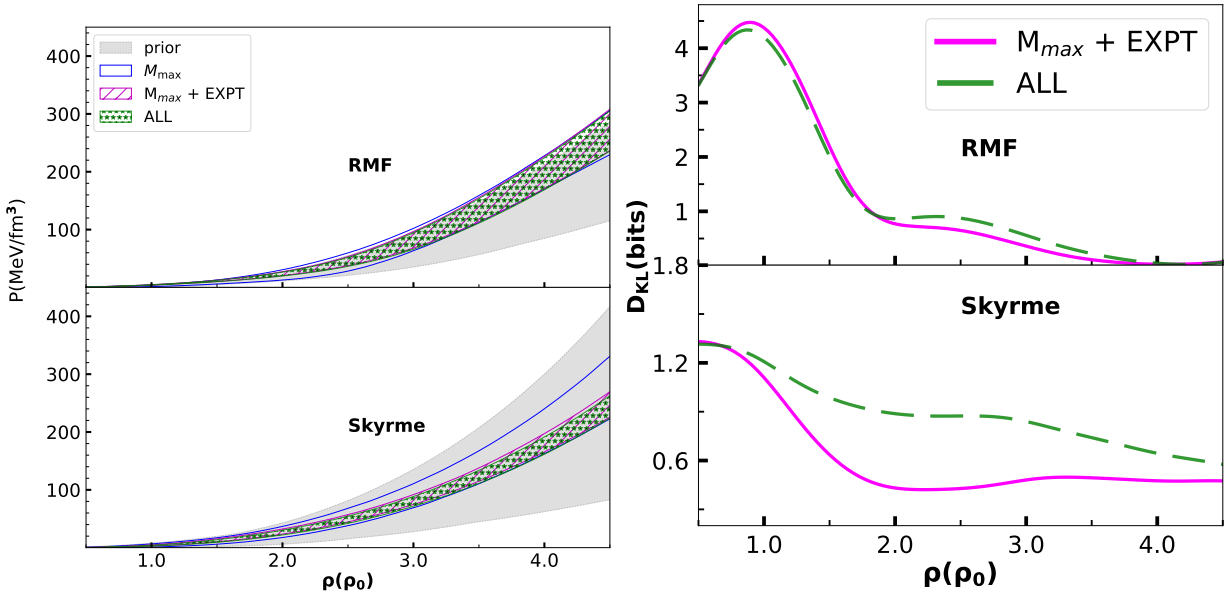

FIG. 3: The 95% confidence intervals for the posterior distributions of the pressure for the neutron star matter as a function of baryon density for the RMF (top) and Skyrme (bottom) mean field models corresponding to different scenarios as indicated(left panel). The variations of Kullback–Leibler divergence (D_{KL}) as a function of baryon density. The values of D_{KL} shown by solid (dashed) line is obtained for the scenario M_{max} + EXPT (ALL) with respect to the prior updated with maximum neutron star mass(right panel).

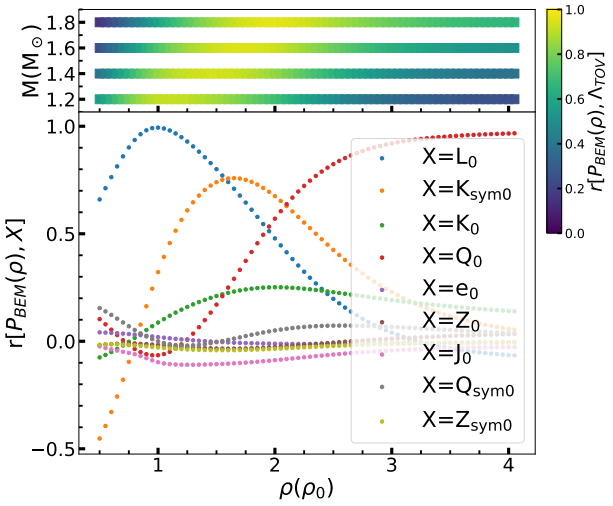

FIG. 4: Plots for the correlations of the β- equilibrium pressure at a given density ($P_{BEM}(\rho)$) with the nuclear matter parameters (lower panel) and with tidal deformability at a given mass $\Lambda_{TOV}(M)$(upper panel). The results are obtained by varying all the nuclear matter parameters considered (see text for detail). Here it is clear that K_0, Q_0, L_0 and K_{sym0} are the most important parameters to model tidal deformability for the NS mass considered.

no constraint (ii) with pure neutron matter (PNM) constraint (iii) associated with the EoSs for which central baryon density for 1.8 $M_\odot$ ($\rho_c(1.8)$) below $3.5\rho_0$ together with the PNM constraint. In the case of PNM constraint those EoSs are selected which satisfy the energy per particle for PNM within 90% confidence interval up to $2\rho_0$ derived from χEFT[16]. The Λ_{func} represents Λ_{l_4}, Λ_{l_9} and $\Lambda_{q_4+l_5}$ for a given NS mass, while Λ_{TOV} values are obtained by varying all the NMPs. The results are plotted in Fig.5 for NS masses 1.2 $M_\odot$ and 1.8 $M_\odot$, respectively for 1000 randomly selected EoSs from our extensive data set corresponding to the cases (ii) and (iii).The functions Λ_{l_9} and $\Lambda_{q_4+l_5}$ are the ones giving less RMSE. In addition the restriction of the central density of the star always $\leq 3.5\rho_0$ comes from the fact that beyond this density it is very likely to have phase transition to non-nucleonic degrees of freedom e.g. hyperons, quarks, hybrid matter, Bose condensate etc, in which cases a direct comparison between properties of finite nuclei with NS observable becomes inappropriate. Therefore after repeating the calculation by excluding these EoSs and the results are presented in the lower panels. It is clear that now the deviations for $\Lambda_{q_4+l_5}$ from Λ_{TOV} for all the EoSs are within 10%.

[1] K. G. Wilson, Phys. Rev. D **10**, 2445 (1974).

[2] P. de Forcrand, arXiv e-prints , arXiv:1005.0539 (2010),

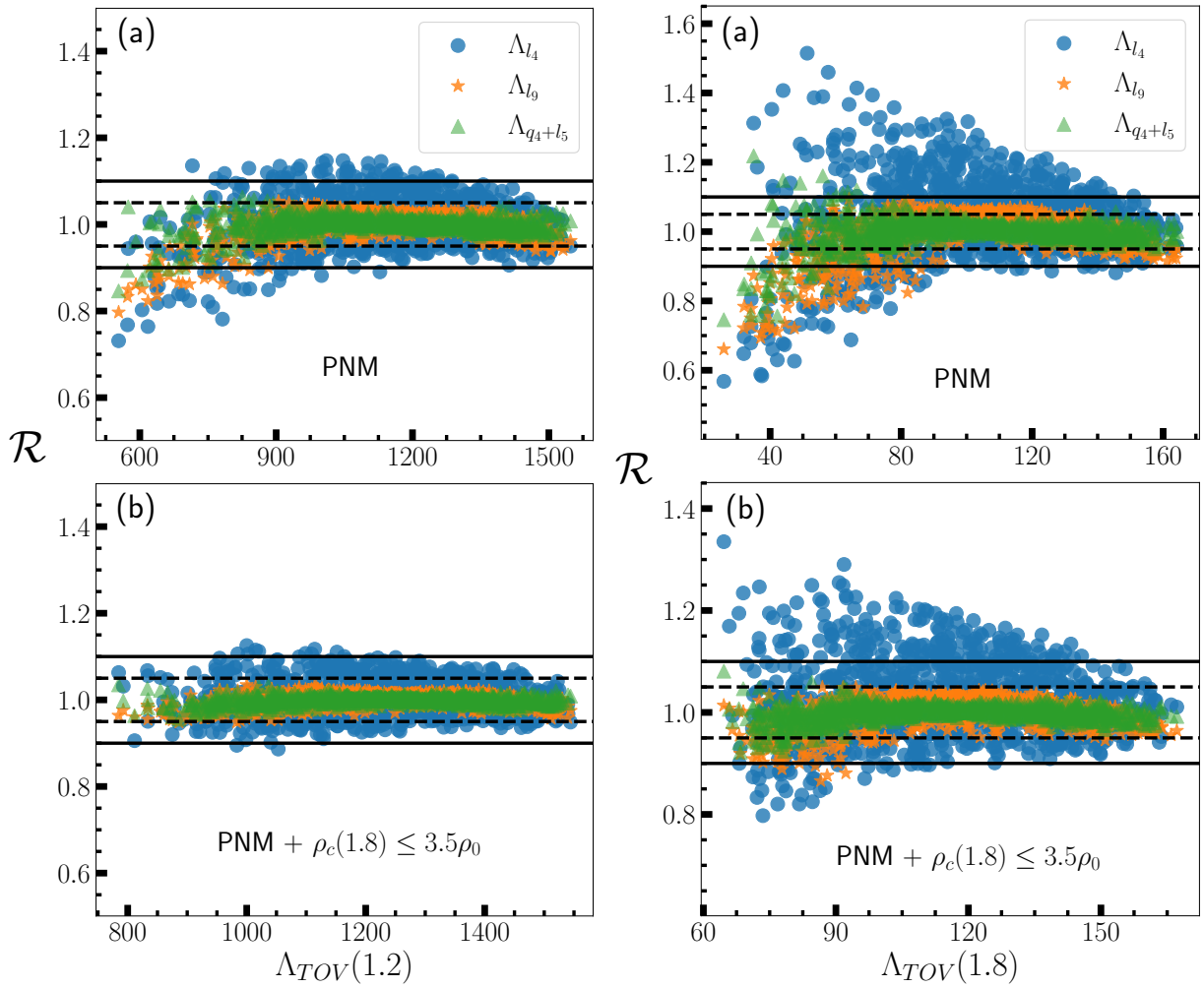

FIG. 5: The ratio $\mathcal{R} = \frac{\Lambda_{TOV}}{\Lambda_{func}}$ for the neutron star mass 1.2 and 1.8 $M_\odot$. The Λ_{TOV} is obtained by varying all the nuclear matter parameters.The results are for 1000 EoSs randomly drawn from a large sample of EoSs. The upper panel corresponds to the NMP set consistent with energy per particle of PNM within 90% confidence interval up to $2\rho_0$ derived from χEFT. The lower panel has an additional constraint on the central density of 1.8 $M_\odot$ NS ($\rho_c(1.8)$) which is below $3.5\rho_0$. The dashed and solid horizontal lines represent 5% and 10% deviations of Λ_{func} from Λ_{TOV}, respectively.

arXiv:1005.0539 [hep-lat] .

[3] J. R. Oppenheimer and G. M. Volkoff, Phys. Rev. **55**, 374 (1939).

[4] G. Baym, T. Hatsuda, T. Kojo, P. D. Powell, Y. Song, and T. Takatsuka, Reports on Progress in Physics **81**, 056902 (2018), arXiv:1707.04966 [astro-ph.HE] .

[5] T. Hinderer, B. D. Lackey, R. N. Lang, and J. S. Read, Phys. Rev. D - Particles, Fields, Gravitation and Cosmology **81**, 123016 (2010).

[6] X. Roca-Maza and N. Paar, Progress in Particle and Nuclear Physics **101**, 96 (2018), arXiv:1804.06256 [nucl-th] .

[7] H. Koehn *et al.*, (2024), arXiv:2402.04172 [astro-ph.HE] .

[8] A. Gómez Nicola, Symmetry **12**, 945 (2020), arXiv:2005.08234 [hep-ph] .

[9] F. Özel and P. Freire, **54**, 401 (2016).

[10] B. A. Freedman and L. D. McLerran, Phys. Rev. D **16**, 1169 (1977).

[11] G. Baym, C. Pethick, and P. Sutherland, Astrophys. J. **170**, 299 (1971).

[12] J. Carriere, C. J. Horowitz, and J. Piekarewicz, Astrophys. J. **593**, 463 (2003).

[13] S. M. A. Imam, N. K. Patra, C. Mondal, T. Malik, and B. K. Agrawal, Phys. Rev. C **105**, 015806 (2022).

[14] S. M. A. Imam, T. Malik, C. Providência, and B. K. Agrawal, (2024), arXiv:2401.06018 [nucl-th] .

[15] S. M. A. Imam, A. Mukherjee, B. K. Agrawal, and G. Banerjee, Phys. Rev. C **109**, 025804 (2024), arXiv:2305.11007 [nucl-th] .

[16] J. Lattimer, Annual Review of Nuclear and Particle Science **71**, 433 (2021).